Journal: Biomechanics and Modeling in Mechanobiology

Mathematical modelling of bone adaptation of the metacarpal subchondral bone in racehorses

Peta L Hitchens[1], Peter Pivonka[2], Fatemeh Malekipour[3], R Chris Whitton[1]

[1] *Equine Centre, Melbourne Veterinary School, Faculty of Veterinary and Agricultural Sciences, University of Melbourne, Werribee, VIC 3030, Australia*

[2] *School of Chemistry, Physics and Mechanical Engineering, Queensland University of Technology, Brisbane, QLD 4000, Australia*

[3] *Department of Biomedical Engineering, University of Melbourne, Parkville, VIC 3010, Australia*

Corresponding author

Peta L Hitchens

Email: phitchens@unimelb.edu.au

Phone: +61 3 8001 2448

ORCID ID: 0000-0002-7528-7056

Key words (4-6)

subchondral bone adaptation, bone volume fraction, multiscale modelling, computational modelling, stress fracture, race horse injury

Acknowledgements

This project is part of the Equine Limb Injury Prevention Research Program funded by Racing Victoria Ltd. (RVL), the Victorian Racing Industry Fund (VRIF) of the Victorian State Government, and the University of Melbourne. The authors thank Chloé Lerebours for providing further information on the square root function outlined in Lerebours *et al.* (2015). Data was contributed by Amy Williamson, Jose Holmes, and Sandra Martig. Sandra Martig was supported by an Australian Government Research Training Program Scholarship.

Nomenclature

Symbol	Definition	Unit
f_{BM}	Bone volume fraction	proportion
S_v	Bone specific surface	mm^{-1}
α	Fraction of bone specific surface	mm^{-1}

E	Bone stiffness	MPa
μ	Osteocyte mechanosensitivity	nmol/(MPa*μm^2)
k_f	Bone formation rate	μm^3/(nmol*day)
τ	Bone formation rate, dependant on ψ_{tissue}	μm^3/(nmol*day)
k_r	Resorption rate	μm^3/(nmol*day)
A_{OCL}	Bone resorption rate via osteoclast activity	μm^3/(nmol*day)
α_f	Fraction of specific surface available for formation	proportion
α_r	Fraction of specific surface available for resorption	proportion
ψ_{tissue}	Strain energy density	MPa
δ	ψ_{tissue} at half-maximal τ	MPa
γ	Sigmoidicity, curve gradient	-
σ_{zz}	Stress-state (applied loading; applied stress)	MPa
ε_{zz}	Strain-state	-
t	Time	days
v	Poisson's ratio	ratio

Abstract

In Thoroughbred racehorses, fractures of the distal limb are commonly catastrophic. Most of these fractures occur due to the accumulation of fatigue damage from repetitive loading, as evidenced by microdamage at the predilection sites for fracture. Adaptation of the bone in response to training loads is important for fatigue resistance. In order to better understand the mechanism of subchondral bone adaptation to its loading environment, we utilised a square root function defining the relationship between bone volume fraction (f_{BM}) and specific surface (S_v) of the subchondral bone of the lateral condyles of the third metacarpal bone (MCIII) of the racehorse; and using this equation, developed a mathematical model of subchondral bone that adapts to loading conditions observed *in vivo*. The model is expressed as an ordinary differential equation (ODE) incorporating a formation rate that is dependent on strain energy density. The loading conditions applied to a selected subchondral region, i.e. volume of interest (VOI) were estimated based on joint contact forces sustained by racehorses in training. For each of the initial conditions of f_{BM} we found no difference between subsequent homeostatic f_{BM} at any given loading condition, but the time to reach equilibrium differed by initial f_{BM} and loading condition. We found that the observed values for f_{BM} from the mathematical model output were a good approximation to the existing *in vivo* data for racehorses in training or at rest. This model provides the basis for understanding the effect of changes to training strategies that may reduce the risk of racehorse injury.

Introduction

Fractures of the distal limb in racehorses are commonly catastrophic (Boden et al. 2006; Rosanowski et al. 2017). Most of these fractures occur, not because of a traumatic incident, but due to the accumulation of fatigue damage of bone from repetitive loading, as evidenced by focal remodelling at the fracture interfaces and microdamage at the predilection sites for fracture (Muir et al. 2008; Riggs et al. 1999a). Subchondral bone injuries are also recognised as being associated with bone material fatigue (Martig et al. 2013), with a high proportion of racehorses (up to 80%) sustaining such injuries (Barr et al. 2009; Pinchbeck et al. 2013; Powell 2012; Riggs et al. 1999a). The relationship between applied load and the fatigue life of bovine cortical and trabecular bone (Bowman et al. 1998; Carter and Hayes 1976), and subchondral bone from racehorses in training (Martig et al. 2013), has been observed to follow a power law function.

Bone is not a static tissue and a complex relationship between bone fatigue injuries and bone's intrinsic processes of modelling and remodelling has been observed (Martig et al. 2014). Bone modelling, commonly referred to as adaption, takes place in response to the stresses experienced

and has been shown to increase the resistance to bone fatigue in both cortical and trabecular bone of rats, humans and bovids (Fatihhi et al. 2015; Rapillard et al. 2006; Warden et al. 2005). Fatigued bone may be removed by remodelling (repair) - the coupled process of bone resorption and formation which can also prolong the fatigue life and therefore increase bone's resistance to injury (Taylor et al. 2004).

Bone volume fraction, often denoted as BV/TV or f_{BM} (for brevity we will refer to as the latter throughout the manuscript), is a key histomorphometrical quantity for characterisation of the bone tissue microstructure (Parfitt et al. 1987), and is an important predictor of its load-bearing capacity (Hernandez et al. 2001; Nazarian et al. 2006; Pothuaud et al. 2002) and its fatigue life (Fatihhi et al. 2015; Rapillard et al. 2006). Changes in f_{BM} of the distal metacarpus of racehorses have been observed at the commencement of, and when horses are rested from race training, as the bone adapts to a change in its loading environment (Boyde and Firth 2005; Holmes et al. 2014). The evolution of f_{BM} has been linked to bone specific surface (S_v), that is, the surface on which bone resorption and formation can occur (Fyhrie and Kimura 1999; Lerebours et al. 2015; Martin 1984; Parfitt et al. 1987). The relationship between f_{BM} and S_v has been investigated in humans and other vertebrates previously based on two dimensional (2D)(Martin 1984) and three dimensional (3D) histological measurements of cortical bone (Fyhrie et al. 1993; Lerebours et al. 2015).

Understanding dynamic longitudinal processes, such as subchondral bone modelling and remodelling using cross-sectional data, is challenging. For this reason mathematical modelling has been used to investigate similar processes in humans (Edwards et al. 2010; Edwards et al. 2009; Taylor et al. 2004). The aim of the current study is to use mathematical modelling to better understand the process of subchondral bone adaptation to different loading environments by assessing changes in f_{BM} of the equine distal metacarpus. To achieve this, we aim to (1) realise an equation defining the relationship between f_{BM} and S_v of the subchondral bone of the lateral condyles of the third metacarpal bone (MCIII) of the racehorse; and then using this equation, (2) develop a mathematical model of subchondral bone modelling and remodelling that responds to the loading environment and produces changes in f_{BM} similar to those observed in horses in race training or at rest. Understanding the effect of changes to inputs in this model will assist in the development of training strategies that reduce the risk of racehorse injury (Martig et al. 2013).

Methods

Data sources

Three datasets were used to define the relationship between f_{BM} and S_v. These were from the studies by (1) Holmes et al. (2014), (2) Martig et al., in press), and (3) Williamson et al. (2017). These studies reported bone microstructural properties obtained from the MCIII of Thoroughbred racehorses that underwent post-mortem examinations at the University of Melbourne (Table 1).

Figure 1 presents the volumes of interest for each study. Data set 1 was 2D data derived from back-scattered scanning electron microscopy (BSEM) images of a single section of the palmar distal MCIII bone at a magnification of x200. Resultant resolution was 0.02 µm. The region of interest (ROI) examined was the lateral condylar subchondral bone to a depth of 8 mm (Holmes et al. 2014). Data set 2 consists of 3D data derived from microCT of 6.7 mm diameter cores drilled from lateral condyles to a depth of 5.1 mm with a resolution of 5 µm. The imaged volume was divided into three VOI from distal to proximal each 1.7 mm in depth (Martig et al., in press). Data set 3 consists of 3D data derived from microCT of medial condyles to a depth of 10mm, 10mm dorsopalmar width and 20 mm lateromedial width. The imaged volume was divided into three volumes of interest (VOI) of equal size from lateral to medial; axial, mid condyle and medial. Imaging was at a resolution of 10 µm (Williamson et al. 2017).

Unlike human subchondral bone which is predominantly trabecular bone with a low f_{BM} typically ranging from 0.2 to 1 (Fyhrie et al. 1993; Lerebours et al. 2015; Martin 1984), the equine subchondral bone at the VOI sites depicted in Figure 1 are subjected to high loads and are more like cortical bone (f_{BM} 0.7 to 1) (Holmes et al. 2014; Whitton et al. 2013; Whitton et al. 2010).

[INSERT FIGURE 1 HERE]

[INSERT TABLE 1 HERE]

Relationship between bone volume fraction and specific surface

Equations 1 and 2 shown below are as per the established system of nomenclature (Dempster et al. 2013; Parfitt et al. 1987) for both 2D and 3D bone structures. Bone volume fraction is defined as the bone volume (BV and B.Ar for 3D and 2D measures, respectively) divided by the tissue volume or total area of interest (TV; T.Ar). There was no requirement to convert measurements of f_{BM} because porosity measurements are equivocal in 2D and 3D (Parfitt et al. 1987) and are not sensitive to image resolution (Slyfield Jr et al. 2009). Thus, it is expressed as:

$$f_{BM} = BV/TV = \frac{B.Ar}{T.Ar} \text{ (–)} \quad (1)$$

Bone specific surface or surface density is defined as the bone surface (BS) for 3D and bone perimeter (B.Pm) for 2D structures, divided by the tissue volume or total area of interest, expressed as:

$$S_v = BS/TV = \frac{B.Pm}{T.Ar} * f(morphology) \text{ (mm}^{-1}\text{)} \quad (2)$$

Where the coefficient expressed by $f(morphology)$ is used to transform the 2D measure into 3D (Lerebours et al. 2015). In studies of cortical and cancellous human bone, this coefficient has been proposed as being equal to ~1, 1.2, or 4/π (Lerebours et al. 2015; Martin 1984; Parfitt et al. 1987). To enable comparison with 3D bone surface measurements, we multiplied 2D S_v by 4/π (1.273), because this value is recognised as the standard conversion (Parfitt et al. 1987). In addition, because the resolution of the data from Martig et al. (in press) was half that of Williamson et al. (2017), dividing the Martig et al. (in press) S_v data by a factor of 2 approximated the data on a similar scale. It is possible that the lower resolution images did not provide a good representation of S_v. Different image processing techniques have been found to improve S_v representation (Slyfield Jr et al. 2009).

In order to realise the relationship between f_{BM} and S_v, we applied and compared three previously defined equations used on human data to the equine data. These were a commonly used fifth-order polynomial equation (Eq.3) described by Martin (1984), a harmonic mean function (Eq.4) described by Fyhrie and Kimura (1999), and a square root function (Eq.5) described by Lerebours et al. (2015).

$$S_v = 0.0323 * (1 - f_{BM}) - 0.0939 * (1 - f_{BM})^2 + 0.134 * (1 - f_{BM})^3 - 0.101 * (1 - f_{BM})^4 + 0.0288 * (1 - f_{BM})^5 \quad (3)$$

$$\frac{1}{S_v} = \frac{1}{1/12.88 * f_{BM}} + \frac{1}{1/29.96 * (1 - f_{BM})'} \quad (4)$$

$$S_v = 11.84 * \sqrt{1 - f_{BM}} * (0.8504 * f_{BM} + 1 - 0.8504) \quad (5)$$

To assess whether alternative equations produced better fitting curves than the previously defined equations for humans, we used the Stata module 'curve fit' (version 4.0) to generate curve estimation statistics and associated plots for 35 different linear and non-linear regression models,

with adjustment for clustering to account for multiple measurements within individual horses, for the relationship between f_{BM} and S_v (Wei 2013). A combination of high r^2, followed by low goodness-of-fit statistics - Akaike (AIC) and Bayesian (BIC) information criterion, and root mean square error (RMSE) of the regression - were used to select and rank the most appropriate model (Hardin et al. 2007). Over-fitted or non-biologically plausible curves were not ranked. The difference between the Lerebours et al. (2015) and Gompertz relation functions was only marginal, and thus we chose to use the Lerebours et al. (2015) square-root function due to its use within the literature for this purpose (see Supplementary Table S1).

Figure 2 presents the previously defined equations using human data, and a new equation fitted to the f_{BM} and S_v data points from this present study of racehorses (Eq.6). The final selected equation for the relationship between f_{BM} and S_v was the square root function, based on that previously described by Lerebours et al. (2015): $S_v = a \cdot \sqrt{1 - f_{BM}} \cdot g(f_{BM})$, where we employ the same constraint f_{BM}=1 at S_v=0 so that $g(f_{BM}) = b \cdot f_{BM} + 1 - b$. The values for the coefficients a and b are obtained from the square-root function regression model fitted to our data. As per Lerebours et al. (2015), we have not included the constraint f_{BM}=0 at S_v=0 because we do not have data in order to understand the nature of the relationship where f_{BM} is less than 0.5 (likely trabecular regions).

$$S_v = 11.42 * \sqrt{1 - f_{BM}} * (-0.02 * f_{BM} + 1 - (-0.02)) \quad (6)$$

Interaction terms were fitted to the selected square root function model to determine whether the relationship between f_{BM} and S_v was modified by study and horse-level factors, where the first part of the equation remains the same (main effect) and the second part includes interaction coefficients (*i, i0, i1*) for each study factor (e.g. where *var*= a binary term for sex):

$$S_v = a \cdot \sqrt{1 - f_{BM}} \cdot g(f_{BM}) + i \cdot var + \left(i0 \cdot var \cdot \sqrt{1 - f_{BM}}\right) \cdot i1 \cdot f_{BM} \cdot var + 1 - i1))$$

All three datasets were different from each other (Supplementary Figure 1; p<0.001). Horses that were in training had lower S_v at lower values of f_{BM} than horses at rest (p<0.001). Bone located most proximal compared to distal (p<0.001), and axial compared to abaxial (p<0.001), had lower S_v at lower values of f_{BM}. No significant interaction effects were observed between male and female horses (male n=153, female n=105; p= 0.085), right and left limbs (right n=137, left n=124; p=0.180), presence or absence of fracture (fracture n=83, no fracture n=178; p=0.063), horses that had raced (raced n=135, unraced n=126; p= 0.985), and terms for age in years (mean 3.25, s.d 1.39; p=0.836), and number of starts (mean 6.67, s.d 12.24; p= 0.561).

Statistical analyses, including linear and non-linear regression modelling, were conducted in Stata/SE 14 (StataCorp. 2015. Stata Statistical Software: Release 14. College Station, TX: StataCorp LP).

[INSERT FIGURE 2 HERE]

Mathematical modelling

Mathematical modelling was conducted in MATLAB R2015b (The MathWorks Inc., Natick, MA, 2000). Modelling was performed in order to ascertain whether different initial conditions of f_{BM} affected the maximum f_{BM} reached, as well as the time taken to reach homeostasis of f_{BM} at different loading conditions. Initial conditions for $f_{BM}(t_0)$ were set at values representative of those observed in previous studies for racehorses in rest and in training. The lowest bone volume fraction (taken from the most distal 43.2 mm of the central shaft of the MCIII sliced in the mediolateral plane) was observed in an untrained two-year-old Thoroughbred horse ($f_{BM}(t_0)$= 0.5)(Boyde and Firth 2005). Effects of initial conditions of f_{BM} were also investigated for values obtained previously for racehorses that had been resting for greater than four weeks ($f_{BM}(t_0)$= 0.8) (Holmes et al. 2014; Whitton et al. 2013), and for those that had been in high-intensity training for at least four weeks ($f_{BM}(t_0)$= 0.9)(Holmes et al. 2014).

The bone modelling and remodelling process is expressed as a multiscale model in an ordinary differential equation (ODE) defined on a respective representative volume element (RVE) of bone. This RVE is comprised of the bone matrix and the pores. The hierarchical structure of the bone (i.e. cell -> tissue -> organ) is accounted for by acknowledging that f_{BM} is lost or gained based on cellular activities and that the bone material (tissue) properties such as stiffness is linked to f_{BM} (Colloca et al. 2014). Because of this, in this section we refer to loading conditions as stress-states because these apply at the tissue-level, whereas load is based on the horse's activity and applies to the organ (bone) level. To express this analytically, we re-write the equation by Colloca et al. (2014), solving for f_{BM} at each incremental point in time. We start with:

$$\frac{df_{BM}}{dt} = k_f * f_{OBL} * \alpha_f * S_v \ - k_r * r_{OCL} * \alpha_r * S_v \quad (7)$$

Where k_f and k_r are the formation and resorption rates; f_{OBL} and r_{OCL} represent frequency of cellular activity of osteoblasts and osteoclasts; and α_f and α_r are the fractions of specific surface available for bone formation and resorption, respectively. We then specify that the fractions of

specific surface available for bone formation and/or resorption events in the RVE are equal, i.e. $\alpha_f = \alpha_r = \alpha$ (Eq.8).

$$\frac{df_{BM}}{dt} = \left(k_f * f_{OBL} - k_r * r_{OCL}\right) * \alpha * S_v \quad (8)$$

Then, continuing to use the same assumptions as Colloca et al. (2014), we adopt the expression for bone formation via osteoblast activity, inclusive of osteocyte mechanosensitivity (μ) but with the addition of a formation rate (τ) that is dependent on strain energy density (ψ_{tissue})(Eq.9).

$$k_f * f_{OBL} = \tau * \mu * \psi_{tissue} \quad (9)$$

The constant bone resorption rate via osteoclast activity is expressed as:

$$k_r * r_{OCL} = A_{OCL} \quad (10)$$

Consequently, we can express the changes in bone volume fraction as:

$$\frac{df_{BM}}{dt} = \left(\tau_{\psi_{tissue}} * \mu * \psi_{tissue} - A_{OCL}\right) * \alpha * S_v \quad (11)$$

Values for model parameters such as osteocyte mechanosensitivity (μ), resorption rate (A_{OCL}) and fraction of specific surface (α) are presented in Table 2. S_v is defined as per Lerebours et al. (2015) square root function described earlier (Eq.6) with parameters optimised to the racehorse data. Note that equation 11 is similar to Colloca et al. (2014) with the exception of the bone formation rate (τ). For humans it was assumed constant, whereas at the extremes of loading to which the racehorse skeleton is exposed, bone formation depends on loading regime. This has been demonstrated in equine cortical bone (Davies 1995; Wang et al. 2016) and is likely to occur in equine subchondral trabecular bone due to the observed formation of woven bone in young horses first introduced to training (Boyde and Firth 2005). Hence, we included a dependency of τ on ψ_{tissue} in equation 11. The sigmoidal function describing this dependency is given in Appendix (Eq.A1).

[INSERT TABLE 2 HERE]

Note that the stress state of subchondral bone in race horses can be determined from 3D finite element calculations. However, performance of the latter is out of scope of the current paper. As a first approximation we assume that the loading of subchondral bone in race horses induces a uniaxial compressive stress state:

$$\sigma_{zz} = \begin{Bmatrix} \sigma_{xx} \\ \sigma_{yy} \\ \sigma_{zz} \\ \sigma_{xy} \\ \sigma_{yz} \\ \sigma_{xz} \end{Bmatrix} = \begin{Bmatrix} 0 \\ 0 \\ \sigma_{zz} \\ 0 \\ 0 \\ 0 \end{Bmatrix} \quad (12)$$

Strain energy density (ψ_{tissue}) was calculated using the equations provided in Colloca et al. (2014) and similar also to Andreaus et al. (2011, 2013), based on the stress-state (σ_{zz}) and strain-state in bone (ε_{zz}). Utilising Hooke's law for a linear isotropic material, bone tissue strain can then be calculated for a given stress-state (Eq.13)(Ugural and Fenster 2003).

$$\begin{Bmatrix} \varepsilon_{xx} \\ \varepsilon_{yy} \\ \varepsilon_{zz} \\ \varepsilon_{xy} \\ \varepsilon_{yz} \\ \varepsilon_{xz} \end{Bmatrix} = \frac{1}{\mathrm{E}} \begin{pmatrix} 1 & -v & -v & 0 & 0 & 0 \\ -v & 1 & -v & 0 & 0 & 0 \\ -v & -v & 1 & 0 & 0 & 0 \\ 0 & 0 & 0 & 2(1+v) & 0 & 0 \\ 0 & 0 & 0 & 0 & 2(1+v) & 0 \\ 0 & 0 & 0 & 0 & 0 & 2(1+v) \end{pmatrix} \begin{Bmatrix} \sigma_{xx} \\ \sigma_{yy} \\ \sigma_{zz} \\ \sigma_{xy} \\ \sigma_{yz} \\ \sigma_{xz} \end{Bmatrix} \quad (13)$$

Where E is the compressive Young's modulus (i.e., tissue stiffness) and v is the Poisson's ratio. Based on equation 13, for strain $\varepsilon_{zz} = \frac{1}{E}\sigma_{zz}$, our strain energy density equation reduces to (Eq.14):

$$\psi_{tissue} = \frac{1}{2E}\sigma_{zz}^2 \quad (14)$$

Bone stiffness is associated with strain rate in both compact and trabecular bone. Carter and Hayes (1977) suggest that the modulus is approximately proportional to the strain rate raised to the 0.06 power (Eq.15). Consequently, according to the feedback mechanostat, as f_{BM} changes at each step of bone tissue loss or gain E_{tissue} also changes and therefore we now have an updated and corresponding strain-state (Andreaus et al. 2012; Andreaus et al. 2014).

$$E_{tissue} = E_0 * \dot{\varepsilon}^{0.06} * {f_{BM}}^3 \quad (15)$$

Where E_0 is the initial compressive modulus (MPa), that is the mean bone stiffness of subchondral bone of the metacarpal condyle in thoroughbreds from Martig et al. (2013), $\dot{\varepsilon}$ is the strain rate (per second), and f_{BM} is the apparent bone density (gr/cm^3).

Table 3 presents strain rates ($\dot{\varepsilon}$) for each stress-state by horse gait. Peak strain rates were calculated for each stress-state ($\dot{\varepsilon}_\sigma$) by dividing the maximum strain (ε_{max}) by time to peak strain (t_σ)(Eq.16).

$$\dot{\varepsilon}_\sigma = \frac{\varepsilon_{max}}{t_\sigma} \quad (16)$$

Time to peak strain occurs approximately at 35% of stance for the walk (Harrison et al. 2010; Harrison et al. 2012; McGuigan and Wilson 2003) and mid-stance for the trot to gallop (Harrison et al. 2010; Harrison et al. 2014; Harrison et al. 2012; Hjertén and Drevemo 1994; McGuigan and Wilson 2003). Speed and stance duration for the walk, trot, and leading leg canter (slow) were based on gait experiments for Thoroughbred horses (Harrison et al. 2012). Stance duration predictions for the canter (6 m/s) and gallop (≥11 m/s) were obtained using the quadratic equation coefficients for pooled lead and non-lead forelimb data from Witte et al. (2006). A hypothetical maximum racehorse speed was estimated at 21 m/s based on the quadratic equation predicting speed from a stress-state of 114 MPa (Table 3). Maximum racehorse speed has been suggested to reach 18 m/s (Witte et al. 2004), and was predicted to potentially reach ~20 m/s with zero limb overlap time (when more than one leg is on the ground)(Witte et al. 2006).

We chose stress-states representative of contact forces in the metacarpal/sesamoid articulation joint during walking, trotting and cantering (Harrison et al. 2014; Riggs et al. 1999b), as well as estimated loads at racing speed (Witte et al. 2006). Stress-states chosen range between 30 MPa (walking) to 114 MPa (maximum racing speed), evaluated at 12 MPa increments. These represent 27-101% of yield stress reported in the lateral condyle of the distopalmer aspect of the MCIII (Rubio-Martínez et al. 2008), and include the stress values previously used to determine compressive fatigue life of metacarpal condylar subchondral bone in racehorses (54, 66, 78, and 90 MPa)(Martig et al. 2013). Contact forces in the metacarpal/sesamoid joint for speeds of 6 m/s approximately translate to a pressure of 48 MPa and at 7 m/s to a pressure of 67 MPa (Martig et al. 2013; Riggs et al. 1999b). Although not confirmed, pressures of greater than 80 MPa are likely representative of those experienced at racing speeds (Martig et al. 2013; Witte et al. 2006).

[INSERT TABLE 3 HERE]

As described in the Appendix, the bone formation rate is dependent on strain energy density, a function of the current stress-state and the level at which the bone is already adapted i.e. the f_{BM}. Osteonal bone formation rates have been reported to be significantly higher for racehorses in training at mid (1.247 μm/day) and high (1.335 μm/day) exercise intensity compared to those at rest (1.094 μm/day)(Firth et al. 2005). In another study, formation rates for horses at rest were as low as 1.2 μm/day compared to horses trained over 40 days at the trot (2.6 μm/day), canter (2.2 μm/day), and gallop (12.7 μm/day)(Davies 1995; Wang et al. 2016). In weanlings, subchondral bone formation rates are as low as 0.5 μm/day for horses in training compared to 0.2 μm/day for horses at rest (Kawcak et al. 2010). Although these studies were missing information on f_{BM} at given loads, which may explain the variability in published results, they give an indication of minimum and maximum values. We chose to set the minimum bone formation rate to 1.094 μm/day (Firth et al. 2005) and the maximum to 12.7 μm/day (Davies 1995; Wang et al. 2016), but excluded the findings from the study of weanlings as they may not be representative of racehorses entering their racing career as 2-year-olds.

Lastly, the rate of change of f_{BM} is dependent on the availability of specific surface that can be modelled (Martin 1984; Pivonka et al. 2013). We estimated the fraction of specific surface from Whitton et al. (2013) based on the average value of eroded surface (E.Pm) plus mineralising surface (Md.Pm) as a percentage of total bone surface (B.Pm). For the lateral condylar subchondral bone this was 19% for racehorses in training that had not sustained a fracture.

Analysis of model behaviour

Differences in model behaviour under different loading and initial conditions of f_{BM} are described. Specifically, we investigated whether the initial conditions of f_{BM} resulted in different maximum or minimum f_{BM} at a given load, the specifications that result in the maximum or minimum f_{BM} achieved, how many days it takes to reach homeostasis at each given load, and whether f_{BM} was similar to what we observe in racehorses in training or at rest given the applied loads. For the latter, we fitted generalised linear regression models with an interaction term between training duration of training period (ordinal; ten day intervals) and a binary variable denoting whether the data were *in vivo* (0) or based on the mathematical model output (1). Statistical significance for all tests was set at $p<0.05$.

Results

Mathematical model behaviour

The relationships between time in days and f_{BM} at differing loads and initial conditions ($f_{BM}(t_0)$ = 0.5, 0.8, and 0.9) are presented in Figure 3. There was no difference in homeostatic f_{BM} for each $f_{BM}(t_0)$ within any given load, however the time taken to reach homeostasis differed.

[INSERT FIGURE 3 HERE]

In an under-loaded state, where f_{BM} is decreasing, the rate of decrease is rapid in the first three to six weeks (21 to 42 days) then slows down as we approach equilibrium. The lower the load the faster f_{BM} decreases although for the $f_{BM}(t_0)$= 0.9 initial condition the initial rate of decrease is lower than the $f_{BM}(t_0)$= 0.8 initial condition due to higher values of f_{BM} resulting in less S_v available for remodelling. For very low intensity exercise (σ ≤ 42 MPa), the model takes up to about ten weeks (72 days) to attain equilibrium. Concurrently, the rapid f_{BM} decrease is driven by the low strain energy density and resultant low formation rate. Table 4 presents the results of the ODE output for time in which the minimum f_{BM}, ψ_{tissue} , τ were reached, i.e. the point at which homeostasis commenced, stratified by f_{BM0} and σ. The minimum f_{BM} at a stress-state of 30 MPa was 0.44; reached at day 31 for an $f_{BM}(t_0)$ of 0.5 and up to day 69 at an $f_{BM}(t_0)$ of 0.9.

[INSERT TABLE 4 HERE]

[INSERT TABLE 5 HERE]

In an overloaded state, where f_{BM} is increasing, the rate of increase is rapid in the first month (30 days) then slows down as we approach equilibrium. For high intensity exercise (σ ≥ 90 MPa), it takes 14 weeks (98 days) or more before equilibrium is attained. Because higher f_{BM} results in lower S_v, the amount of S_v available for remodelling decreases. Concurrently, the slowdown in f_{BM} increase is also driven by an increase in bone stiffness which in turn decreases strain state, strain energy density and thus formation rate. Lastly, the bone formation rate is much slower for higher initial f_{BM} conditions purely because the amount of S_v available for remodelling is less. In Table 5 we present the results of the ODE output for time in which the maximum f_{BM}, ψ_{tissue} , τ were reached, stratified by f_{BM0} and σ. The maximum f_{BM} at a stress-state of 114 MPa was 1.00; reached at day 162 for an $f_{BM}(t_0)$ of 0.5, and at day 148 for an $f_{BM}(t_0)$ of 0.9.

The lowest values of strain energy density (ψ_{tissue}=0.31 MPa) and formation rate (τ =0.00159 μm^3/(nmol*day) were observed at the highest $f_{BM}(t_0)$ and the lowest stress-state (30

MPa); while conversely the highest values of strain energy density (ψ_{tissue}=21.65 MPa) and formation rate (τ =0.00986 μm^3/(nmol*day) were observed at the lowest $f_{BM}(t_0)$ and the highest stress-state (114 MPa) (Tables 4 and 5).

Comparison between model and in vivo data

Using pooled data from the three previous *in vivo* studies, racehorses at rest had a mean lateral condyle f_{BM} of 0.86 (95% CI 0.83, 0.88; n=60), significantly lower than racehorses in training (0.92; 95% CI 0.91, 0.92; n=177; p<0.001). There was no significant difference in the observed values for f_{BM} from the mathematical model output compared to the *in vivo* data for racehorses in training (p=0.469) or at rest (p=0.921)(Figures 4 and 5).

[INSERT FIGURE 4 HERE]

[INSERT FIGURE 5 HERE]

Discussion

We present a mathematical model of bone turnover derived from principles of bone behaviour and microstructural data from the subchondral bone of racehorses that can predict observed changes in bone volume fraction in racehorses in race training and at rest. Additionally, a square root function based on that by Lerebours et al. (2015) was confirmed that defined the relationship between bone volume fraction and specific surface of the subchondral bone of the lateral condyles of the MCIII of the racehorse. Adaptation to high-intensity training loads may take about 14 weeks (98 days) in previously adapted bone, and longer in bone from horses that have never trained. Complete adaptation due to rest may take between four and ten weeks for low to high initial conditions, respectively.

Similar multiscale mathematical models to predict adaptation changes by modifying cell-level or tissue-level parameters and assessing their effects of disuse and/or exercise at the organ level have been developed and reviewed elsewhere (Webster and Müller 2011). Our model is an analytical model that unlike finite element (FE) based models does not take tissue architecture or detailed strain energy density distribution into account. However analytical models have been demonstrated to produce similar results to FE based models with less computational time. For example, Colloca et al. (2014) developed a multiscale analytical formulation of bone remodelling to predict bone density in children, with our model being largely based on a similar analytical solution. As well as reducing

computational time considerably, their mathematical model provided reasonable predictions of bone volume fraction at equilibrium compared to a more complex and time consuming micro-finite element (FE) model, with differences between the models ranging from 14% for increased (200%) loading to 0.6% for decreased (50%) loading (Colloca et al. 2014). A key difference between our models and others has been the timeframe in which changes are observed – days, weeks or months rather than years (Colloca et al. 2014; Ruimerman et al. 2005); due to the much smaller applied daily stresses in comparison to the extremely large contact forces observed in the racehorse (Harrison et al. 2014). Nevertheless, our models behaved similarly to other multiscale models where increased loads resulted in bone gain while reduced loads result in bone loss, and the greatest changes occurred most rapidly at the commencement of a change in loading conditions (Colloca et al. 2014; Ruimerman et al. 2005).

The relationship between bone volume fraction and specific surface of the subchondral bone of the lateral condyles of the MCIII of the racehorse was found to best fit the square root equation proposed by Lerebours et al. (2015). Likewise, we found that our data did not fit as well to the previously described fifth-order polynomial (Martin 1984) and harmonic mean (Fyhrie and Kimura 1999) equations. As foreseen by Lerebours et al. (2015), the fifth-order polynomial presented with 'spurious oscillations' at low bone volume fractions, and thus was not found to be biologically plausible. Our square root equation shows that as the bone volume fraction increases, the unit change in specific bone surface is greater. The differences in the bone volume fraction and specific surface relationship curves between the studies may be due to, for example, the inclusion of both healthy and diseased samples (e.g. osteomalacia, osteogenesis imperfecta, and osteoporosis)(Martin 1984). The samples from the present study were assumed to be healthy, as they were obtained from racehorses that had raced, or were being prepared to race.

In the current study the relationship between bone volume fraction and specific surface was modified by study (Supplementary Figure 1), sample location, and training status. However, these differences in curves were most notable only at the lower end of bone volume fraction values, where data points were sparse and thus were not deemed to be important for prediction of bone specific surface for racehorses in training because f_{BM} values lower than 0.8 are rarely observed. Lerebours et al. (2015) suggested that the relationship between bone volume fraction and bone specific surface may be subject-specific as sex and pore density affected the relationship between bone volume fraction and specific surface in human cortical bone, but was not found to be modified by body height, weight or age. Sex was not a significant modifier in our study, and we had only

limited data on pore density. Inclusion of racehorses with atypical bone volume fraction, and multiple measurements from the same subjects over time, may be necessary to confirm these findings.

The model suggests that a young horse entering training could substantially adapt its subchondral bone to high-intensity training within the first month. But such a sudden increase in loading in unadapted bone would risk the rapid accumulation of microdamage. Experimentally, trabecular bone with lower bone volume fraction can sustain fewer number of cycles to failure (Fatihhi et al. 2015). In practice, the introduction of training in an inexperienced athlete is performed incrementally so that adaptation can occur for each level of loading, without the risk of injury, before progressing to the next level of loading (Gabbett et al. 2016).

Adaptation to rest with lower levels of loading follows a similar, though initially more gradual, timeline to that of adaption to exercise in our model. Although the bone resorption rate remained constant, the rate of bone volume fraction reduction increases as the bone surface available for resorption increases, until increasing strain energy density again slows this reduction in bone volume fraction. In our model, horses with an initial bone volume fraction of 0.90 take 20% longer (66 days) to reach homeostasis at the lowest simulated load (30 MPa) compared to horses starting at 0.80 (55 days). This suggests that horses with very high bone volume fraction (i.e. those that have undergone more intensive training), and (consequently) low bone specific surface, will get less benefit from the same period of rest in terms of bone turnover than horses with lower bone volume fraction.

Bone volume fraction predicted by our model was a good approximation of *in vivo* values reported for racehorses in training and at rest. Higher bone volume fraction has been attributed to deposition of new bone and a decrease in, or little indication of, bone resorption observed in racehorses in training (Boyde and Firth 2005; Holmes et al. 2014; Murray et al. 2001; Whitton et al. 2013). For racehorses in training, maximal bone formation occurs at high load regions predisposed to injury (e.g dorsal radial, medial third carpal)(Murray et al. 2001), and it is subsequently those horses with greater bone volume that are more likely to sustain a fracture (Whitton et al. 2013).

There are several limitations of this study that should be considered. Transformation of specific surface from 2D to 3D requires assumptions on the 3D geometry of the pores (Lerebours et al. 2015; Martin 1984). Osteocyte mechanosensitivity was assumed to be 1 nmol/(MPa·μm^2) in the adult racehorse. However Colloca et al. (2014) found that changes in osteocyte mechanosensitivity had an

effect on predicted bone volume fraction, finding a 12% difference in bone volume fraction when osteocyte mechanosensitivity was increased by 200%, and a 10% difference when it was decreased by 50%. Osteocyte mechanosensitivity is driven by hormonal regulators or bone degenerative diseases, thus it may differently affect growing (or older) racehorses. The mechanical loading conditions were simple uniaxial and are in reality more complex (Fatihhi et al. 2016), but a good first approximation. The model was developed by inputting average values for bone stiffness, and singular minimum and maximum bone formation and resorption rates from previous studies. When using average input values, computational models do not always produce average results (Cook and Robertson 2016), thus caution should be taken when interpreting these findings as they may not be entirely representative of the racehorse population. We conducted a sensitivity analysis by varying input factors (initial condition, stress-state) to determine their influence on model results. We recommend subsequent development of models consider Monte Carlo simulation, drawing randomly from larger datasets for all model input parameters, rather than using only mean or maximum values as model inputs. Studies have shown that bone resorption is reduced during a progressively intense training program (Murray et al. 2001), therefore dynamic resorption rate should be considered in future models. The model also does not include damage accumulation due to rigorous exercise. Lastly, our model used data at varying time points during racehorses' training preparations; but we did not have longitudinal data for each individual during their preparations because data were collected at post-mortem. Ideally models need to be validated against longitudinal data, but this is both time consuming, costly, and potentially unethical.

We confirmed an equation defining the relationship between bone volume fraction and specific surface of the subchondral bone of the lateral condyles of the MCIII of the racehorse; and using this equation, developed a mathematical model of modelling and remodelling that responds to the loading environment and produces changes in bone volume fraction similar to those observed *in vivo*. This model provides the basis for understanding the effect of changes to training strategies that may reduce the risk of racehorse injury. For example, the model shows that bone loss can be quite rapid with the cessation of race training, so that even with rest periods as short as ten days, careful reintroduction of training is subsequently required to allow readaptation. Future studies should refine this model to consider the addition of damage accumulation and alteration of loading condition over time to better mirror racehorse training programs. This will allow more directly applicable recommendations on the introduction of training to be made. The model can then also be used to determine the effect of different training programs on changes to bone volume fraction in order to reduce risk of stress fracture.

Appendix

Sigmoidal function

We approximated the sigmoidal function equation from Peterson and Riggs (2010) to represent the relationship between ψ_{tissue} and formation rate (τ)(Eq.A1; Figure 6). Formation rates do not differ significantly for racehorses in lower intensity exercise (i.e. walk to canter), but are higher when unadapted bone is subjected to high-intensity exercise. $H^{+}_{\psi_{tissue}}$ represents the hyperbolic term (H) for the stimulus variable (ψ_{tissue}) with an increase (+) from steady-state. Included terms are for sigmoidicity (γ) that specifies the curve gradient, maximum estimated formation rate (τ_{max}), minimum estimated formation rate (τ_{min}), and the estimated value of ψ_{tissue} that produces the half-maximal formation rate ($\delta = 7$). The latter value was estimated from the maximum value of ψ_{tissue} at ultimate failure of the equine metacarpus, which has been reported to be about 14 MPa (Les et al. 1994).

$$H^{+}_{\psi_{tissue}} = \tau_{min} + \frac{(\tau_{max} - \tau_{min}) * {\psi_{tissue}}^{\gamma}}{\delta^{\gamma} + {\psi_{tissue}}^{\gamma}} \quad \text{(A1)}$$

[INSERT FIGURE 6 HERE]

TABLES

Table 1. Summary of three studies reporting bone microstructural properties of the lateral condyles of the MCIII of Thoroughbred racehorses, stratified by volume of interest.

No.	Study	Dimension	Method	Resolution	VOI	N	f_{BM}	S_v [a]
				µm			mean ± s.d.	mean ± s.d.
1	Holmes et al. (2014)	2D	BSEM	0.02	-	48	0.88 ± 0.06	4.22 ± 2.78
2	Martig et al. (in press)	3D	MicroCT	5	distal	40	0.96 ± 0.02	5.07 ± 1.20
					mid	40	0.94 ± 0.03	5.77 ± 1.09
					proximal	40	0.89 ± 0.06	6.45 ± 0.95
					all	120	0.93 ± 0.05	5.76 ± 1.22
3	Williamson et al. (2017)	3D	MicroCT	10	axial	31	0.91 ± 0.06	3.43 ± 1.13
					mid	31	0.91 ± 0.05	3.25 ± 0.86
					medial	31	0.82 ± 0.07	4.20 ± 0.87
					all	93	0.88 ± 0.07	3.63 ± 1.04
	All studies combined	3D	n/a	n/a	all	261	0.90 ± 0.07	4.72 ± 1.84

[a] Data reported as 2D measurements (B.Pm/T.Ar) were transformed into 3D by multiplying by a factor of $4/\pi$ (1.273)(Parfitt et al. 1987).

Table 2. Parameters in the mathematical models of bone adaptation.

Parameter	Definition	Unit	Value	Reference
$f_{BM}(t_0)$	Bone volume fraction, initial condition	proportion	0.5:0.8:0.9	Boyde and Firth (2005); Whitton et al. (2013)
E_0	Bone stiffness, initial condition	MPa	2500 ± 494	Martig et al. (2013)
E_{max}	Bone stiffness, maximum	MPa	5608.3	Malekipour (unpublished)
μ	Osteocyte mechanosensitivity	nmol/(MPa*μm^2)	1	Colloca et al. (2014)
A_{OCL}	Bone resorption rate, time constant	μm^3/(nmol*day)	0.011	Boyde and Firth (2005)
τ_{min}	Bone formation rate, minimum	μm^3/(nmol*day)	0.001094	Firth et al. (2005)
τ_{max}	Bone formation rate, maximum	μm^3/(nmol*day)	0.0127	Davies (1995); Wang et al. (2016)
τ_{half}	Bone formation rate, half maximal	μm^3/(nmol*day)	0.005803	n/a
δ	ψ_{tissue} at half-maximal formation rate	MPa	7	Les et al. (1994)
γ	Sigmoidicity, curve gradient	-	1	-
α	Fraction of specific surface	mm^{-1}	0.19	Whitton et al. (2013)
σ_z	Applied loading (stress-state)	MPa	30:114	Martig et al. (2013); Riggs et al. (1999b); Rubio-Martínez et al. (2008); Witte et al. (2006)
t_0	Time at point zero, initial condition	time (days)	0	n/a
t_{end}	Time at end point, final condition	time (days)	365	n/a

Table 3. Estimated strain rate ($\dot{\varepsilon}$) for each stress-state (loading condition; joint contact pressure), derived from stance duration, time to peak strain, and peak strain, by horse gait and approximate speed for Thoroughbreds in training.

Gait	Speed (m/sec)	Stiffness (MPa) at f_{BM}=0.90	Representative joint contact pressure (MPa)	Stance duration (sec)	Peak strain (ε_{max})	Time to peak strain (sec)	Strain rate ($\dot{\varepsilon}$; sec^{-1})
Walk	1.4[a]	1441	30	0.740[c]	0.0053	0.259	0.02
Trot	3.6[a]	1523	42	0.290[c]	0.0075	0.145	0.05
Trot/canter transition	6[b]	1605	54	0.156[d]	0.0096	0.078	0.12
Canter	7.5[a]	1626	66	0.160[c]	0.0118	0.080	0.15

Gallop	11[b]	1681	78	0.107[d]	0.0139	0.054	0.26
Race speed	14[b]	1714	90	0.089[d]	0.0160	0.045	0.36
Race speed	17[a]	1740	102	0.079[d]	0.0182	0.040	0.46
Max. speed	21[b]	1750	114	0.080[d]	0.0203	0.040	0.51

[a] Estimated speeds from published studies (Harrison et al. 2014; Martig et al. 2013; Riggs et al. 1999b; Witte et al. 2006); [b] Predicted speed using the quadratic equation: speed (m/s) = 0.001*σ_{zz}^2 + 0.0843*σ_{zz} - 1.6555; [c] Mean stance duration from Harrison et al. (2012); [d] Predicted stance duration using the quadratic equation from Witte et al. (2006): (0.4591*speed^2 – 17.426*speed + 243.56)/1000; Peak strain = (1/E_{max})*load; Time to peak strain = stance duration*proportion at which peak strain occurs. For walk this proportion is 0.35, and for trot or faster this occurs at mid-stance (0.50); Strain rate = peak strain / time to peak strain. [e] Predicted stiffness (E_{tissue}) at $f_{BM} = 0.90$ using equation 14.

Table 4. The minimum bone volume fraction (f_{BM}) reached and the time in days, strain energy density (ψ_{tissue}), and formation rate (τ) at which it is reached (representing commencement of equilibrium), by initial $f_{BM}(t_0)$ and stress-state (σ). Minimum f_{BM} occurs on day 0 in instances where bone is over-loaded (*italics*).

	$f_{BM}(t_0)$ = 0.5					$f_{BM}(t_0)$ = 0.8					$f_{BM}(t_0)$ = 0.9				
σ	**Time** (days)	**Min.** f_{BM}	S_v (mm^{-1})	ψ_{tissue} (MPa)	**τ** (μm^3/(nmol*day))	**Time** (days)	**Min.** f_{BM}	S_v (mm^{-1})	ψ_{tissue} (MPa)	**τ** (μm^3/(nmol*day))	**Time** (days)	**Min.** f_{BM}	S_v (mm^{-1})	ψ_{tissue} (MPa)	**τ** (μm^3/(nmol*day))
30	31	0.44	8.62	2.60	0.00424	59	0.44	8.62	2.60	0.00424	69	0.44	8.62	2.60	0.00424
42	*0*	*0.50*	8.17	*3.38*	*0.00487*	59	0.55	7.77	2.59	0.00423	72	0.55	7.77	2.59	0.00423
54	*0*	*0.50*	8.17	*5.30*	*0.00609*	71	0.63	6.97	2.60	0.00424	85	0.63	6.97	2.60	0.00424
66	*0*	*0.50*	8.17	*7.81*	*0.00721*	62	0.72	6.06	2.59	0.00423	83	0.72	6.06	2.59	0.00423
78	*0*	*0.50*	8.17	*10.55*	*0.00807*	20	0.80	5.16	2.60	0.00423	93	0.80	5.16	2.60	0.00423
90	*0*	*0.50*	8.17	*13.78*	*0.00879*	*0*	*0.80*	5.13	*3.36*	*0.00486*	95	0.87	4.10	2.60	0.00424
102	*0*	*0.50*	8.17	*17.44*	*0.00938*	*0*	*0.80*	5.13	*4.26*	*0.00548*	*0*	*0.90*	3.62	*2.99*	*0.00457*
114	*0*	*0.50*	8.17	*21.65*	*0.00986*	*0*	*0.80*	5.13	*5.29*	*0.00609*	*0*	*0.90*	3.62	*3.71*	*0.00512*

Table 5. The maximum bone volume fraction (f_{BM}) reached and the time in days, strain energy density (ψ_{tissue}), and formation rate (τ) at which it is reached (representing commencement of equilibrium), by $f_{BM}(t_0)$ and stress-state (σ). Maximum f_{BM} occurs on day 0 in instances where bone is under-loaded (*italics*).

	$f_{BM}(t_0)$ = 0.5					$f_{BM}(t_0)$ = 0.8					$f_{BM}(t_0)$ = 0.9				
σ	**Time** (days)	**Max.** f_{BM}	S_v (mm^{-1})	ψ_{tissue} (MPa)	**τ** (μm^3/(nmol*day))	**Time** (days)	**Max.** f_{BM}	S_v (mm^{-1})	ψ_{tissue} (MPa)	**τ** (μm^3/(nmol*day))	**Time** (days)	**Max.** f_{BM}	S_v (mm^{-1})	ψ_{tissue} (MPa)	**τ** (μm^3/(nmol*day))
30	*0*	*0.50*	8.17	*1.82*	*0.00349*	*0*	*0.80*	5.13	*0.44*	*0.00179*	*0*	*0.90*	3.62	*0.31*	*0.00159*
42	37	0.55	7.77	2.59	0.00423	*0*	*0.80*	5.13	*0.82*	*0.00232*	*0*	*0.90*	3.62	*0.58*	*0.00198*
54	45	0.63	6.97	2.60	0.00424	*0*	*0.80*	5.13	*1.29*	*0.00290*	*0*	*0.90*	3.62	*0.91*	*0.00243*
66	81	0.72	6.06	2.59	0.00423	*0*	*0.80*	5.13	*1.91*	*0.00358*	*0*	*0.90*	3.62	*1.34*	*0.00296*
78	90	0.80	5.16	2.60	0.00423	*0*	*0.80*	5.13	*2.58*	*0.00422*	*0*	*0.90*	3.62	*1.81*	*0.00348*
90	113	0.87	4.10	2.60	0.00424	100	0.87	4.10	2.60	0.00424	*0*	*0.90*	3.62	*2.36*	*0.00402*
102	159	0.94	2.73	2.60	0.00424	152	0.94	2.73	2.60	0.00424	130	0.94	2.73	2.60	0.00424
114	162	1.00	0.00	2.71	0.00433	157	1.00	0.00	2.71	0.00433	148	1.00	0.00	2.71	0.00433

FIGURE CAPTIONS

Figure 1. Volumes of interest (VOI) sampled from the distal metacarpal bone for each of the three studies at the following regions: (a) lateral condyle trabecular and subchondral bone (Holmes et al. 2014), (b) dense subchondral bone of the lateral condyle (Martig et al., in press), and (c) medial condyle trabecular and subchondral bone (Williamson et al. 2017). Image taken by back-scattered scanning electron microscopy (BSEM).

Figure 2. Relationship between bone volume fraction and specific surface. Overlaid curves represent a fifth-order polynomial equation (Martin 1984), a harmonic mean function (Fyhrie et al. 1993), and a square root function (Lerebours et al. 2015) fitted to data from previous studies of humans, and a square root function with 95% confidence intervals, fitted to the adjusted lateral condyle MCIII data from the present study in racehorses (n=261).

Figure 3. The relationship between time in days and bone volume fraction at differing loads (30 to 114 MPa), stratified by initial condition for bone volume fraction: (a) $f_{BM}(t_0)$ = 0.50; (b) $f_{BM}(t_0)$ = 0.80; $f_{BM}(t_0)$ = 0.90.

Figure 4. Comparison between mathematical model output and *in vivo* data from racehorses in training (n=177). Model output includes bone volume fraction (f_{BM}) and 95% confidence intervals observed at stress-states inducing overloading where data for $f_{BM}(t_0)$ =0.8 and 0.9 are pooled.

Figure 5. Comparison between mathematical model output and real-world data from racehorses at rest (n=60). Model output includes bone volume fraction (f_{BM}) and 95% confidence intervals observed at stress-states inducing under-loading where data for $f_{BM}(t_0)$ =0.8 and 0.9 are pooled.

Figure 6. Relationship between strain energy density (ψ_{tissue}) and formation rate (τ), expressed as a hyperbolic function with sigmoidicity ($\gamma = 1$). Minimal and maximum formation rates respectively: 0.001094 (τ_{min}) and 0.0127 (τ_{max}). ψ_{tissue} at the half-maximal formation rate (δ) was set to 7.

SUPPLEMENTARY FILES

Supplementary Table 1. Linear and non-linear regression statistics for the relationship between bone volume fraction and bone specific surface from previously fitted curves and from the Stata module 'curve fit', using N=261 observations from three studies of lateral condyles of the third metacarpus of Thoroughbred racehorses.

Supplementary Figure 1. Relationship between bone volume fraction and specific surface for three studies reporting bone material properties of the lateral condyle of the third metacarpus from Thoroughbred racehorses. Data has been adjusted.

Funding: This study is part of the Equine Limb Injury Prevention Research Program funded by Racing Victoria Ltd. (RVL), the Victorian Racing Industry Fund (VRIF) of the Victorian State Government, and the University of Melbourne.

Conflict of Interest: P.L. Hitchens is employed under the Equine Limb Injury Prevention Research Program and supported by funding from Racing Victoria Ltd. (RVL), the Victorian Racing Industry Fund (VRIF) of the Victorian State Government, and the University of Melbourne. R.C. Whitton is the lead investigator of the Equine Limb Injury Prevention Research Program. P. Pivonka and F. Malekipour have no conflict of interests.

References

Andreaus U, Colloca M, Iacoviello D (2012) An optimal control procedure for bone adaptation under mechanical stimulus Control Engineering Practice 20:575-583

Andreaus U, Colloca M, Iacoviello D (2013) Modeling of trabecular architecture as result of an optimal control procedure. In: Biomedical imaging and computational modeling in biomechanics. Springer, pp 19-37

Andreaus U, Colloca M, Iacoviello D (2014) Optimal bone density distributions: numerical analysis of the osteocyte spatial influence in bone remodeling Computer methods and programs in biomedicine 113:80-91

Andreaus U, Colloca M, Iacoviello D, Pignataro M (2011) Optimal-tuning PID control of adaptive materials for structural efficiency Structural and Multidisciplinary Optimization 43:43-59

Barr E, Pinchbeck G, Clegg P, Boyde A, Riggs C (2009) Post mortem evaluation of palmar osteochondral disease (traumatic osteochondrosis) of the metacarpo/metatarsophalangeal joint in Thoroughbred racehorses Equine Vet J 41:366-371

Boden LA et al. (2006) Risk of fatality and causes of death of Thoroughbred horses associated with racing in Victoria, Australia: 1989–2004 Equine Vet J 38:312-318 doi:10.2746/042516406777749182

Bowman S, Guo X, Cheng D, Keaveny T, Gibson L, Hayes W, McMahon T (1998) Creep contributes to the fatigue behavior of bovine trabecular bone J Biomech Eng 120:647-654

Boyde A, Firth EC (2005) Musculoskeletal responses of 2-year-old Thoroughbred horses to early training. 8. Quantitative back-scattered electron scanning electron microscopy and confocal fluorescence microscopy of the epiphysis of the third metacarpal bone NZ Vet J 53:123-132 doi:10.1080/00480169.2005.36489

Carter DR, Hayes WC (1976) Fatigue life of compact bone: I effects of stress amplitude, temperature and density J Biomech 9:IN7-34 doi:10.1016/0021-9290(76)90136-6

Carter DR, Hayes WC (1977) The compressive behavior of bone as a two-phase porous structure J Bone Joint Surg 59:954-962

Colloca M, Blanchard R, Hellmich C, Ito K, van Rietbergen B (2014) A multiscale analytical approach for bone remodeling simulations: linking scales from collagen to trabeculae Bone 64:303-313

Cook DD, Robertson DJ (2016) The generic modeling fallacy: Average biomechanical models often produce non-average results! J Biomech 496:3609-3615

Davies HMS (1995) The adaptive response of the equine metacarpus to locomotory stress. Doctoral dissertation. University of Melbourne, Australia.,

Dempster DW et al. (2013) Standardized Nomenclature, Symbols, and Units for Bone Histomorphometry: A 2012 Update of the Report of the ASBMR Histomorphometry Nomenclature Committee J Bone Miner Res 28:2-17 doi:10.1002/jbmr.1805

Edwards BW, Taylor D, Rudolphi TJ, Gillette JC, Derrick TR (2010) Effects of running speed on a probabilistic stress fracture model Clin Biomech 25:372-377 doi:http://dx.doi.org/10.1016/j.clinbiomech.2010.01.001
Edwards WB, Taylor D, Rudolphi TJ, Gillette JC, Derrick TR (2009) Effects of stride length and running mileage on a probabilistic stress fracture model Med Sci Sports Exerc 41:2177-2184 doi:10.1249/MSS.0b013e3181a984c4
Fatihhi SJ, Harun MN, Abdul Kadir MR, Abdullah J, Kamarul T, Öchsner A, Syahrom A (2015) Uniaxial and Multiaxial Fatigue Life Prediction of the Trabecular Bone Based on Physiological Loading: A Comparative Study Ann Biomed Eng 43:2487-2502 doi:10.1007/s10439-015-1305-8
Fatihhi SJ, Rabiatul AAR, Harun MN, Kadir MRA, Kamarul T, Syahrom A (2016) Effect of torsional loading on compressive fatigue behaviour of trabecular bone J Mech Behav Biomed 54:21-32 doi:http://dx.doi.org/10.1016/j.jmbbm.2015.09.006
Firth E, Rogers C, Doube M, Jopson N (2005) Musculoskeletal responses of 2-year-old Thoroughbred horses to early training. 6. Bone parameters in the third metacarpal and third metatarsal bones NZ Vet J 53:101-112
Fyhrie DP, Fazzalari N, Goulet R, Goldstein S (1993) Direct calculation of the surface-to-volume ratio for human cancellous bone J Biomech 26:955-967
Fyhrie DP, Kimura JH (1999) Cancellous bone biomechanics J Biomech 32:1139-1148 doi:10.1016/S0021-9290(99)00114-1
Gabbett TJ, Hulin BT, Blanch P, Whiteley R (2016) High training workloads alone do not cause sports injuries: how you get there is the real issue Br J Sports Med 50:444-445
Hardin JW, Hilbe JM, Hilbe J (2007) Generalized linear models and extensions. Stata press,
Harrison SM, Whitton RC, Kawcak CE, Stover SM, Pandy MG (2010) Relationship between muscle forces, joint loading and utilization of elastic strain energy in equine locomotion J Exp Bio 213:3998-4009
Harrison SM, Whitton RC, Kawcak CE, Stover SM, Pandy MG (2014) Evaluation of a subject-specific finite-element model of the equine metacarpophalangeal joint under physiological load J Biomech 47:65-73
Harrison SM, Whitton RC, King M, Haussler KK, Kawcak CE, Stover SM, Pandy MG (2012) Forelimb muscle activity during equine locomotion J Exp Bio 215:2980-2991
Hernandez C, Beaupre G, Keller T, Carter D (2001) The influence of bone volume fraction and ash fraction on bone strength and modulus Bone 29:74-78
Hjertén G, Drevemo S (1994) Semi-quantitative analysis of hoof-strike in the horse J Biomech 27:997-1004 doi:http://dx.doi.org/10.1016/0021-9290(94)90216-X
Holmes J, Mirams M, Mackie E, Whitton R (2014) Thoroughbred horses in race training have lower levels of subchondral bone remodelling in highly loaded regions of the distal metacarpus compared to horses resting from training Vet J 202:443-447
Kawcak CE, McIlwraith CW, Firth EC (2010) Effects of early exercise on metacarpophalangeal joints in horses Am J Vet Res 71:405-411
Lerebours C, Thomas C, Clement J, Buenzli P, Pivonka P (2015) The relationship between porosity and specific surface in human cortical bone is subject specific Bone 72:109-117
Les CM, Keyak JH, Stover SM, Taylor KT, Kaneps AJ (1994) Estimation of material properties in the equine metacarpus with use of quantitative computed tomography J Orthop Res 12:822-833 doi:10.1002/jor.1100120610
Martig S, Chen W, Lee PVS, Whitton RC (2014) Bone fatigue and its implications for injuries in racehorses Equine Vet J 46:408-415 doi:10.1111/evj.12241
Martig S, Lee PVS, Anderson GA, Whitton RC (2013) Compressive fatigue life of subchondral bone of the metacarpal condyle in thoroughbred racehorses Bone 57:392-398 doi:http://dx.doi.org/10.1016/j.bone.2013.09.006
Martin RB (1984) Porosity and specific surface of bone Crit Rev Biomed Eng 10:179-222

McGuigan MP, Wilson AM (2003) The effect of gait and digital flexor muscle activation on limb compliance in the forelimb of the horse Equus caballus J Exp Biol 206:1325-1336 doi:10.1242/jeb.00254
Muir P, Peterson AL, Sample SJ, Scollay MC, Markel MD, Kalscheur VL (2008) Exercise-induced metacarpophalangeal joint adaptation in the Thoroughbred racehorse J Anat 213:706-717 doi:10.1111/j.1469-7580.2008.00996.x
Murray R, Vedi S, Birch H, Lakhani K, Goodship A (2001) Subchondral bone thickness, hardness and remodelling are influenced by short-term exercise in a site-specific manner J Orthop Res 19:1035-1042
Nazarian A, Stauber M, Zurakowski D, Snyder BD, Müller R (2006) The interaction of microstructure and volume fraction in predicting failure in cancellous bone Bone 39:1196-1202
Parfitt AM et al. (1987) Bone histomorphometry: standardization of nomenclature, symbols, and units: report of the ASBMR Histomorphometry Nomenclature Committee J Bone Miner Res 2:595-610
Peterson MC, Riggs MM (2010) A physiologically based mathematical model of integrated calcium homeostasis and bone remodeling Bone 46:49-63
Pinchbeck G, Clegg P, Boyde A, Riggs C (2013) Pathological and clinical features associated with palmar/plantar osteochondral disease of the metacarpo/metatarsophalangeal joint in Thoroughbred racehorses Equine Vet J 45:587-592
Pivonka P, Buenzli PR, Scheiner S, Hellmich C, Dunstan CR (2013) The influence of bone surface availability in bone remodelling—a mathematical model including coupled geometrical and biomechanical regulations of bone cells Engineering Structures 47:134-147
Pothuaud L, Van Rietbergen B, Mosekilde L, Beuf O, Levitz P, Benhamou CL, Majumdar S (2002) Combination of topological parameters and bone volume fraction better predicts the mechanical properties of trabecular bone J Biomech 35:1091-1099
Powell SE (2012) Low-field standing magnetic resonance imaging findings of the metacarpo/metatarsophalangeal joint of racing Thoroughbreds with lameness localised to the region: A retrospective study of 131 horses Equine Vet J 44:169-177 doi:10.1111/j.2042-3306.2011.00389.x
Rapillard L, Charlebois M, Zysset PK (2006) Compressive fatigue behavior of human vertebral trabecular bone J Biomech 39:2133-2139
Riggs C, Whitehouse G, Boyde A (1999a) Pathology of the distal condyles of the third metacarpal and third metatarsal bones of the horse Equine Vet J 31:140-148
Riggs CM, Whitehouse GH, Boyde A (1999b) Structural variation of the distal condyles of the third metacarpal and third metatarsal bones in the horse Equine Vet J 31:130-139 doi:10.1111/j.2042-3306.1999.tb03806.x
Rosanowski S, Chang Y, Stirk A, Verheyen K (2017) Descriptive epidemiology of veterinary events in flat racing Thoroughbreds in Great Britain (2000 to 2013) Equine Vet J 49:2042-3306
Rubio-Martínez LM, Cruz AM, Gordon K, Hurtig MB (2008) Mechanical properties of subchondral bone in the distal aspect of third metacarpal bones from Thoroughbred racehorses Am J Vet Res 69:1423-1433
Ruimerman R, Hilbers P, Van Rietbergen B, Huiskes R (2005) A theoretical framework for strain-related trabecular bone maintenance and adaptation J Biomech 38:931-941
Slyfield Jr CR et al. (2009) Three-dimensional surface texture visualization of bone tissue through epifluorescence-based serial block face imaging J Microsc 236:52-59 doi:10.1111/j.1365-2818.2009.03204.x
Taylor D, Casolari E, Bignardi C (2004) Predicting stress fractures using a probabilistic model of damage, repair and adaptation J Orthop Res 22:487-494
Ugural AC, Fenster SK (2003) Advanced strength and applied elasticity. Prentice Hall, New Jersey, USA

Wang X, Thomas CDL, Clement JG, Das R, Davies H, Fernandez JW (2016) A mechanostatistical approach to cortical bone remodelling: an equine model Biomech Model Mechanobiol 15:29-42 doi:10.1007/s10237-015-0669-x

Warden SJ, Hurst JA, Sanders MS, Turner CH, Burr DB, Li J (2005) Bone adaptation to a mechanical loading program significantly increases skeletal fatigue resistance J Bone Miner Res 20:809-816

Webster D, Müller R (2011) In silico models of bone remodeling from macro to nano—from organ to cell Wiley Interdisciplinary Reviews: Systems Biology and Medicine 3:241-251

Wei L (2013) CURVEFIT: Stata module to produces curve estimation regression statistics and related plots between two variables for alternative curve estimation regression models. Statistical Software Components S457136, Boston College Department of Economics. Boston, USA.

Whitton RC, Mirams M, Mackie EJ, Anderson GA, Seeman E (2013) Exercise-induced inhibition of remodelling is focally offset with fatigue fracture in racehorses Osteoporos Int 24:2043-2048 doi:10.1007/s00198-013-2291-z

Whitton RC, Trope GD, Ghasem-Zadeh A, Anderson GA, Parkin TDH, Mackie EJ, Seeman E (2010) Third metacarpal condylar fatigue fractures in equine athletes occur within previously modelled subchondral bone Bone 47:826-831 doi:http://dx.doi.org/10.1016/j.bone.2010.07.019

Williamson A, Sims NA, Thomas CDL, Lee PVS, Stevenson M, Whitton RC (2017) Biomechanical testing of the calcified metacarpal articular surface and its association with subchondral bone microstructure in Thoroughbred racehorses Equine Vet J doi:10.1111/evj.12748

Witte T, Knill K, Wilson A (2004) Determination of peak vertical ground reaction force from duty factor in the horse (Equus caballus) J Exp Biol 207:3639-3648

Witte TH, Hirst CV, Wilson AM (2006) Effect of speed on stride parameters in racehorses at gallop in field conditions J Exp Biol 209:4389-4397 doi:10.1242/jeb.02518

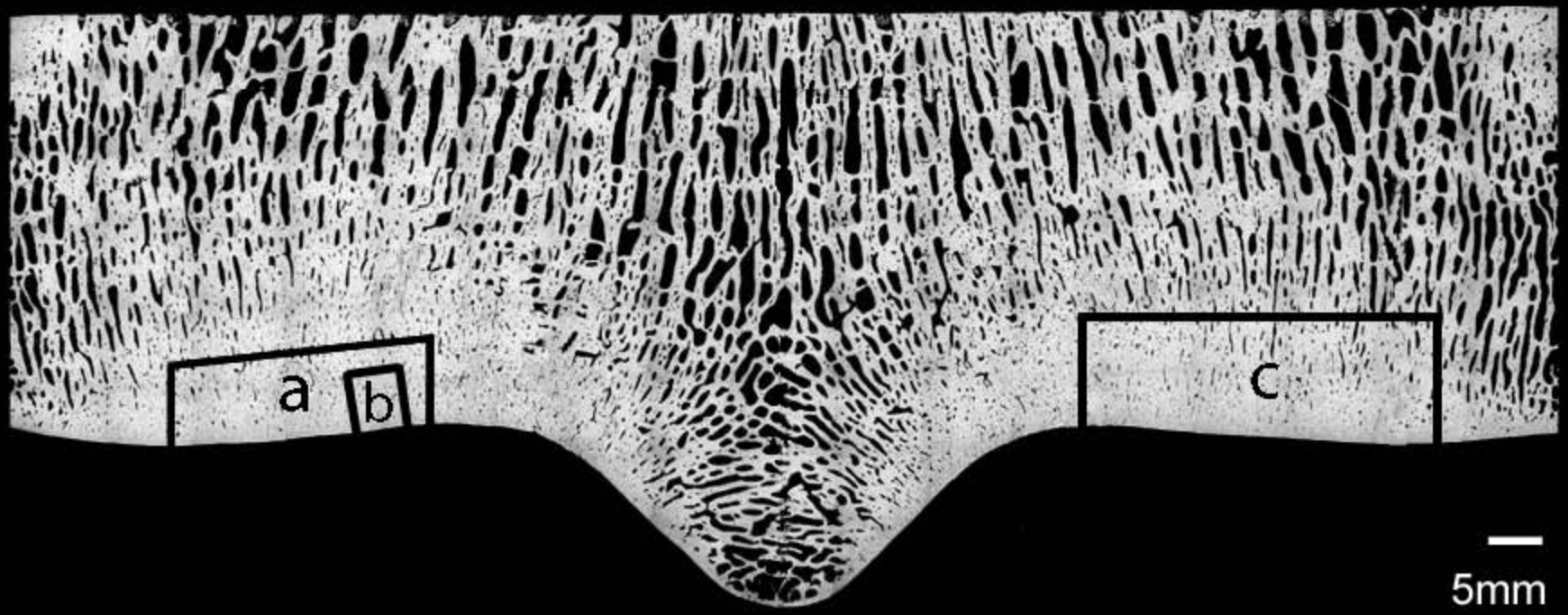
Lat
Med
a
b
c
5mm

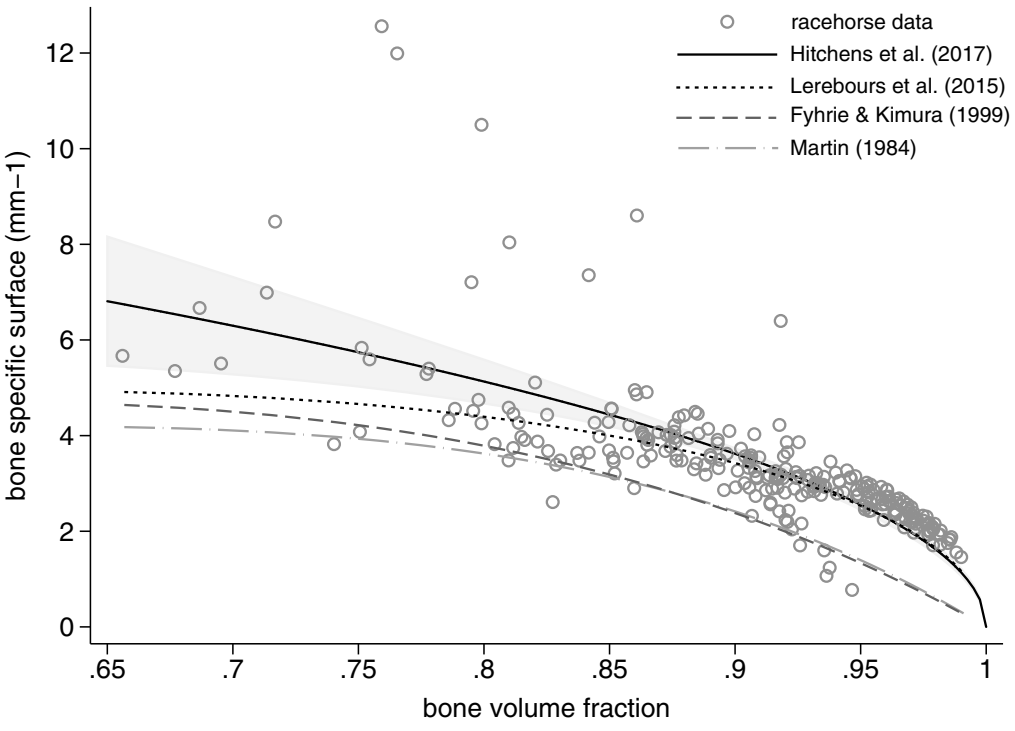
racehorse data
Hitchens et al. (2017)
Lerebours et al. (2015)
Fyhrie & Kimura (1999)
Martin (1984)
bone specific surface (mm−1)
0
2
4
6
8
10
12
.65
.7
.75
.8
.85
.9
.95
1
bone volume fraction

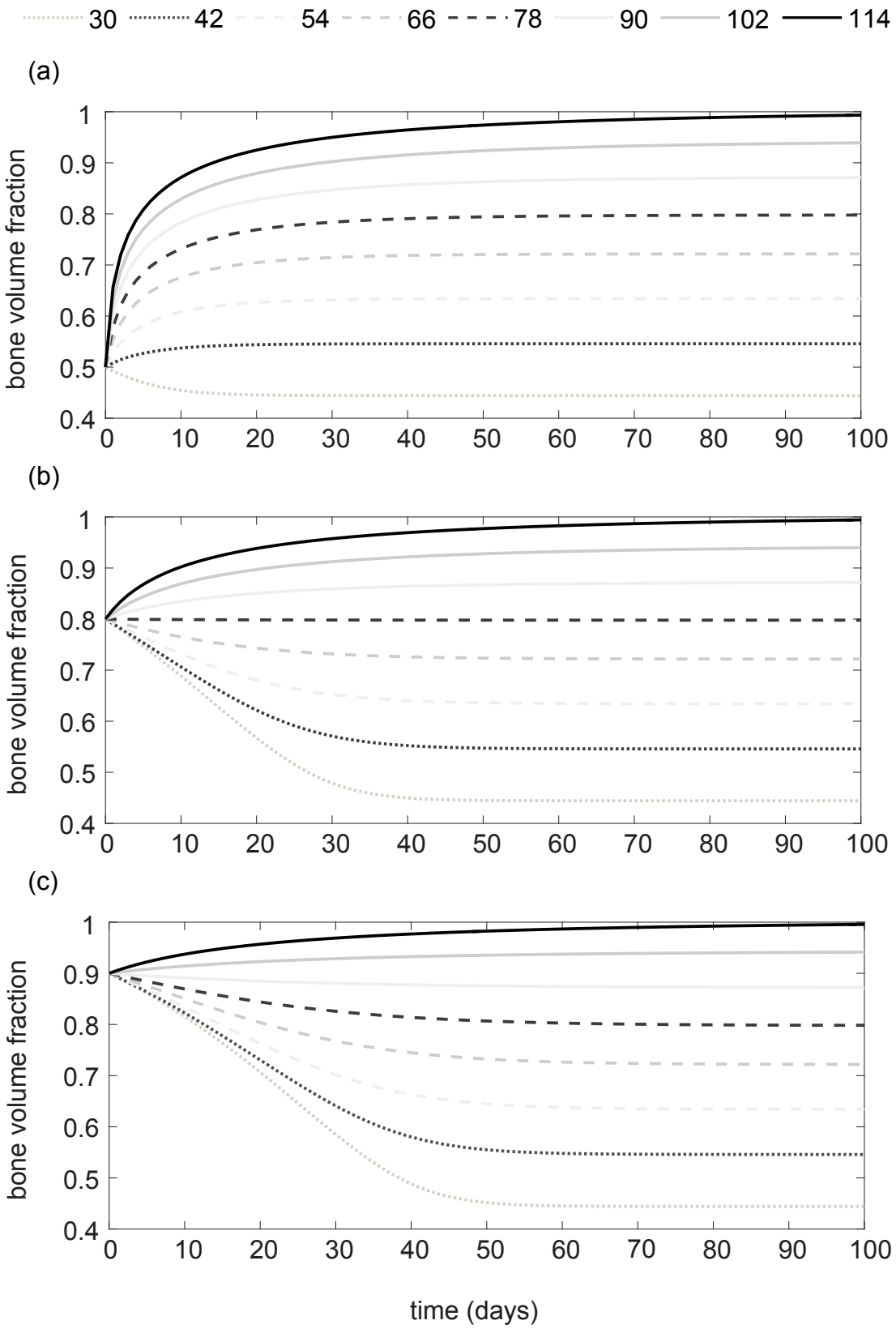
30
42
54
66
78
90
102
114
(a)
(b)
(c)
bone volume fraction
time (days)
0.4
0.5
0.6
0.7
0.8
0.9
1
0
10
20
30
40
50
60
70
80
90
100

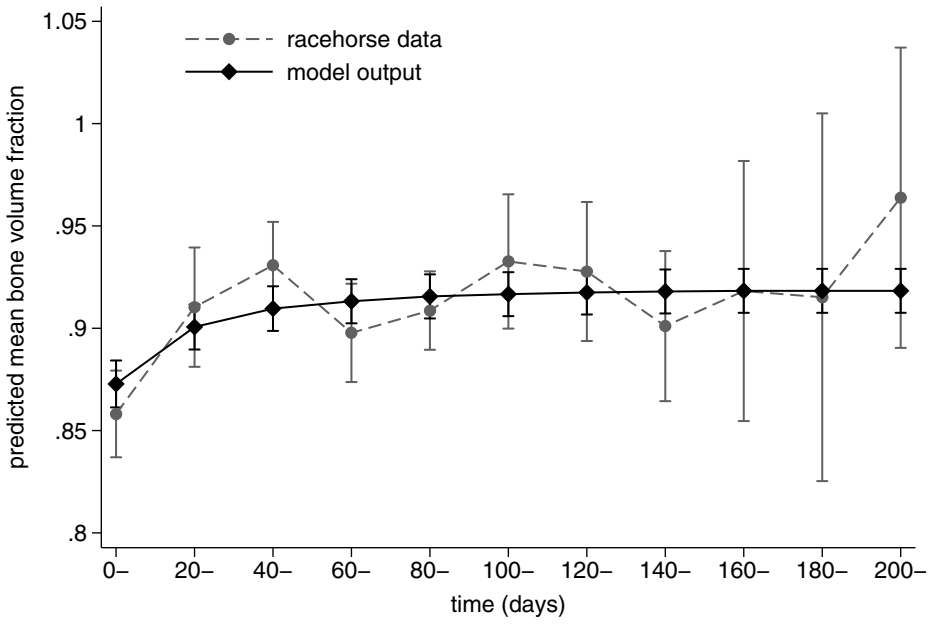
racehorse data
model output
predicted mean bone volume fraction
1.05
1
.95
.9
.85
.8
0–
20–
40–
60–
80–
100–
120–
140–
160–
180–
200–
time (days)

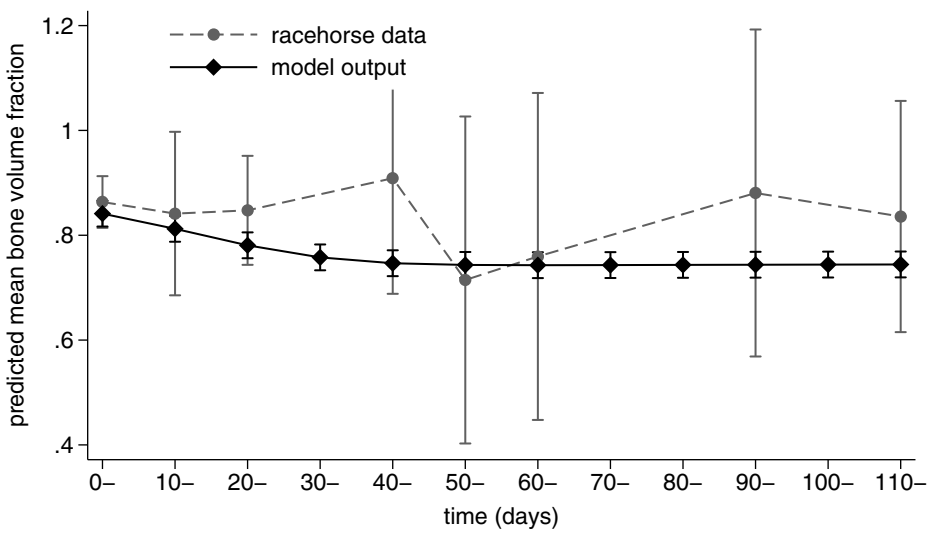
racehorse data
model output
predicted mean bone volume fraction
1.2
1
.8
.6
.4
0–
10–
20–
30–
40–
50–
60–
70–
80–
90–
100–
110–
time (days)

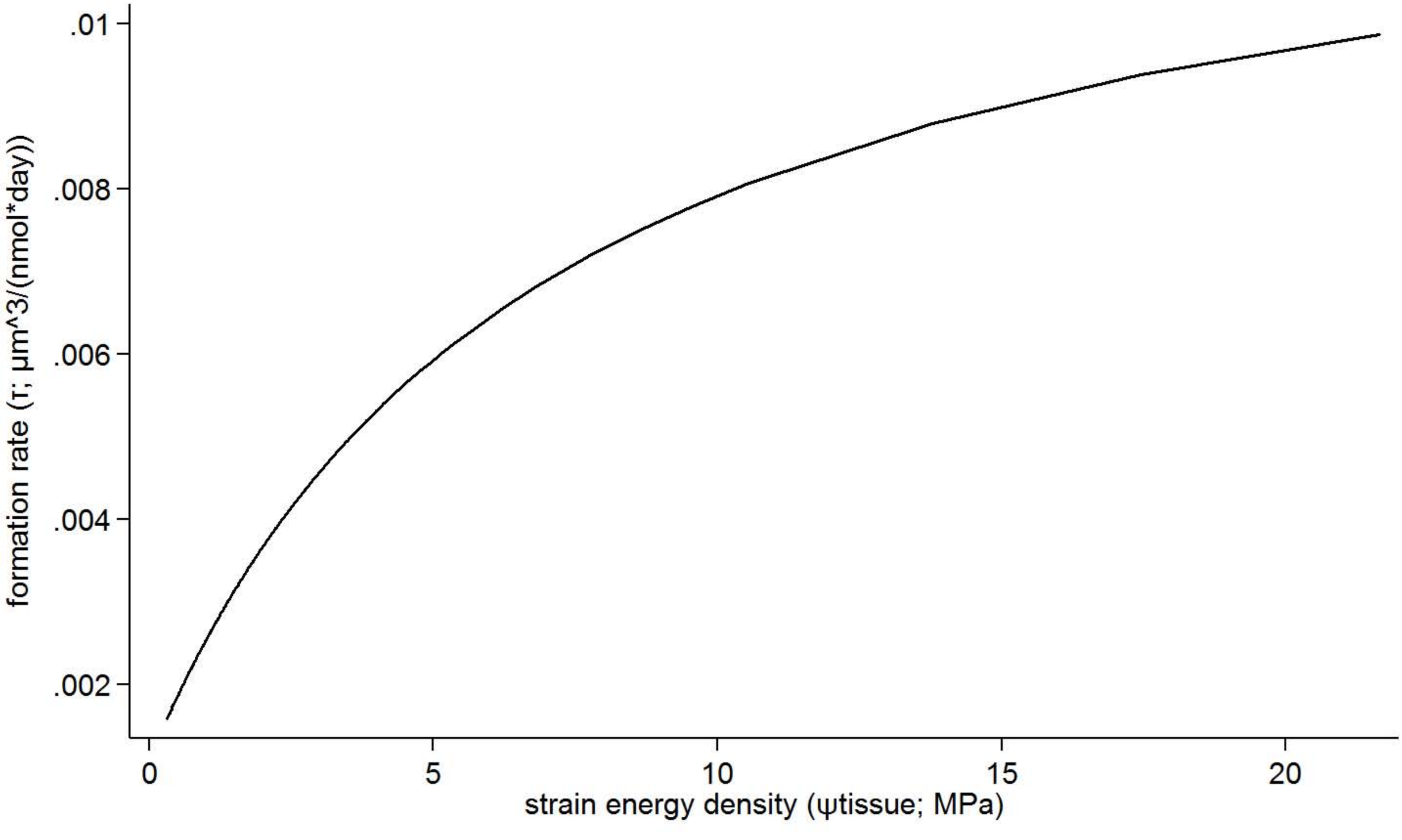
.01
.008
.006
.004
.002
formation rate (τ; μm^3/(nmol*day))
0
5
10
15
20
strain energy density (ψtissue; MPa)

Journal: Biomechanics and Modeling in Mechanobiology

Mathematical modelling of bone adaptation of the metacarpal subchondral bone in racehorses

Peta L Hitchens[1], Peter Pivonka[2], Fatemeh Malekipour[3], R Chris Whitton[1]

[1] *Equine Centre, Faculty of Veterinary and Agricultural Sciences, University of Melbourne, Werribee, VIC 3030, Australia*

[2] *School of Chemistry, Physics and Mechanical Engineering, Queensland University of Technology, Brisbane, QLD 4000, Australia*

[3] *Department of Mechanical Engineering, University of Melbourne, Parkville, VIC 3010, Australia*

Corresponding author

Peta L Hitchens

Email: phitchens@unimelb.edu.au

Phone: +61 3 8001 2448

Supplementary Figure 1. Relationship between bone volume fraction and specific surface for three studies reporting bone material properties of the lateral condyle of the third metacarpus from Thoroughbred racehorses. Data has been adjusted.

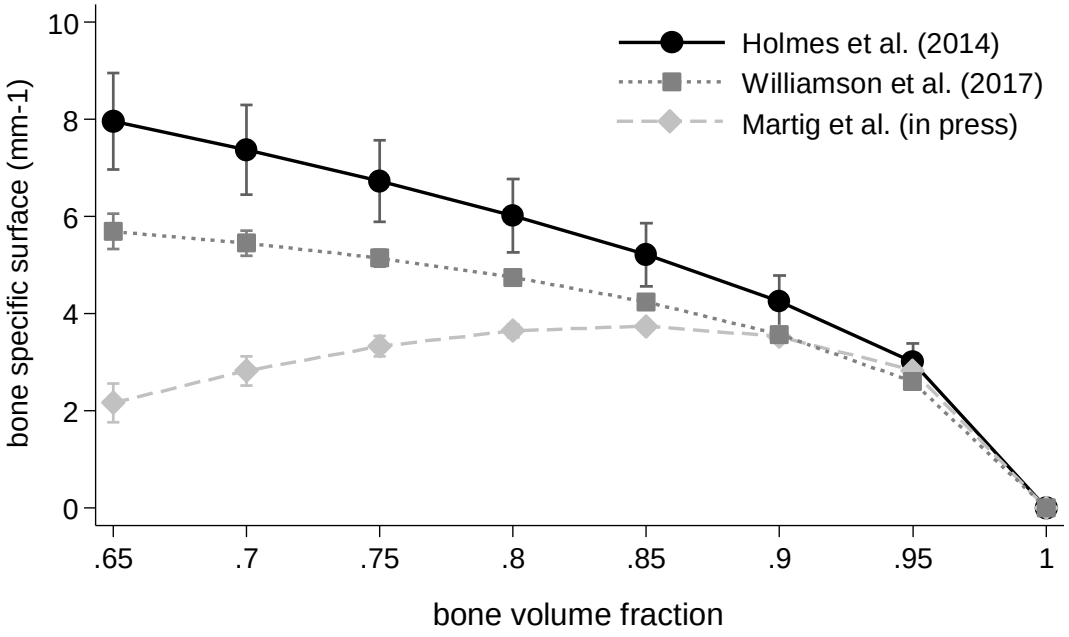

Journal: Biomechanics and Modeling in Mechanobiology

Mathematical modelling of bone adaptation of the metacarpal subchondral bone in racehorses

Peta L Hitchens[1], Peter Pivonka[2], Fatemeh Malekipour[3], R Chris Whitton[1]

[1] *Equine Centre, Faculty of Veterinary and Agricultural Sciences, University of Melbourne, Werribee, VIC 3030, Australia*

[2] *School of Chemistry, Physics and Mechanical Engineering, Queensland University of Technology, Brisbane, QLD 4000, Australia*

[3] *Department of Mechanical Engineering, University of Melbourne, Parkville, VIC 3010, Australia*

Corresponding author

Peta L Hitchens

Email: phitchens@unimelb.edu.au

Phone: +61 3 8001 2448

Supplementary Table 1. Linear and non-linear regression statistics for the relationship between bone volume fraction and bone specific surface from previously fitted curves and from the Stata module 'curve fit', using N=261 observations from three studies of lateral condyles of the third metacarpus of Thoroughbred racehorses.

Model	R^2	RMSE	AIC	BIC	Overfitting or bias	Selection rank
Previously fitted models						
Lerebours et al. (2015)	0.93	1.01	743.11	750.22	No	1
Fyhrie & Kimura (1999)	0.91	1.11	790.11	797.22	No	3
Martin (1984)	0.56	0.97	724.40	742.19	Yes	-
Stata curvefit models						
Gompertz relation	0.93	0.99	732.45	743.12	No	2
Quadratic (constrained)	0.90	1.17	817.29	824.40	No	4
Quadratic (unconstrained)	0.55	0.99	539.48	560.82	No	6
Heat capacity	0.55	0.99	732.79	743.46	No	5
Cubic	0.56	0.99	731.51	745.74	Yes	-
Rational	0.93	0.98	726.56	740.78	Yes	-
Linear	0.55	0.99	554.14	571.93	Yes	-
Bleasdale	0.92	1.03	750.21	757.32	Yes	-
Harris	0.93	0.99	730.95	741.62	Yes	-
MMF	0.93	0.99	732.69	746.92	Yes	-
Weibull	0.56	0.98	730.67	744.90	Yes	-
Sinusoidal	0.55	0.99	731.98	746.21	Yes	-
Gaussian	0.93	0.98	730.14	740.81	Yes	-
Logarithmic	0.54	1.00	735.20	742.32	Yes	-
Inverse	0.53	1.01	740.63	747.74	Yes	-
Power	0.92	1.05	761.01	768.12	Yes	-
S-curve	0.92	1.07	773.60	780.72	Yes	-
Vapor pressure	0.93	0.98	727.72	738.39	Yes	-
Growth	0.92	1.03	750.20	757.32	Yes	-
Exponential	0.92	1.03	750.20	757.32	Yes	-
Geometric	0.93	1.01	739.65	746.77	Yes	-
Modified geometric	0.91	1.10	784.90	792.01	Yes	-
4^{th} order polynomial	0.57	0.97	722.40	736.63	Yes	-
Saturation-growth rate	0.90	1.16	813.92	821.03	Yes	-

Compound	0.92	1.03	750.20	757.32	Yes	-
Logistic	dnc	1.47	935.53	939.08	-	-
Reciprocal logarithmic	0.91	1.13	800.18	807.29	Yes	-
Modified power	0.92	1.03	750.20	757.32	Yes	-
Shifted power	dnc	-	-	-	-	-
Hoerl	0.56	0.98	725.23	728.78	Yes	-
Modified Hoerl	0.93	0.98	727.72	738.39	Yes	-
Reciprocal	0.91	1.10	786.50	793.61	Yes	-
Reciprocal quadratic	0.93	0.98	726.22	736.89	Yes	-
Exponential association	dnc	1.47	935.53	939.08	-	-
Three-parameter exponential	dnc	-	-	-	-	-
association Richards	dnc	1.47	935.53	939.08	-	-

Note: Models that did not converge (dnc), overfitted, biased or non-biologically plausible curves were not ranked.

Author/s:
Hitchens, PL; Pivonka, P; Malekipour, F; Whitton, RC

Title:
Mathematical modelling of bone adaptation of the metacarpal subchondral bone in racehorses

Date:
2018-06-01

Citation:
Hitchens, P. L., Pivonka, P., Malekipour, F. & Whitton, R. C. (2018). Mathematical modelling of bone adaptation of the metacarpal subchondral bone in racehorses. BIOMECHANICS AND MODELING IN MECHANOBIOLOGY, 17 (3), pp.877-890. https://doi.org/10.1007/s10237-017-0998-z.